Research Paper

LncRNA *PMAT–PtoMYB46* module represses *PtoMATE* and *PtoARF2* promoting Pb²⁺ uptake and plant growth in poplar

Panfei Chen [a,b,c], Yuepeng Song [a,b], Xin Liu [a,b], Liang Xiao [a,b], Chenhao Bu [a,b], Peng Liu [a,b], Lei Zhao [a,b], Pär K. Ingvarsson [d], Harry X. Wu [e], Yousry A. El-Kassaby [f], Deqiang Zhang [a,b,c,*]

[a] National Engineering Laboratory for Tree Breeding, College of Biological Sciences and Technology, Beijing Forestry University, No. 35, Qinghua East Road, Beijing 100083, PR China
[b] Key Laboratory of Genetics and Breeding in Forest Trees and Ornamental Plants, College of Biological Sciences and Technology, Beijing Forestry University, No. 35, Qinghua East Road, Beijing 100083, PR China
[c] School of Landscape Architecture, Beijing University of Agriculture, Beijing 102206, PR China
[d] Linnean Center for Plant Biology, Department of Plant Biology, Swedish University of Agricultural Sciences, Box 7080, SE-750 07 Uppsala, Sweden
[e] Umeå Plant Science Centre, Department of Forest Genetics and Plant Physiology, Swedish University of Agricultural Science, Umeå, Sweden
[f] Department of Forest and Conservation Sciences, Faculty of Forestry, The University of British Columbia, Vancouver, British Columbia V6T 1Z4, Canada

HIGHLIGHTS

- Pb²⁺-induced lncRNAs mainly regulate energy metabolism and signal transduction.
- LncRNA *PMAT* and *PtoMYB46* modulate Pb²⁺ uptake in poplar.
- *PtoMYB46* targets *PtoARF2* to positively regulate plant growth.
- Overexpression of *PtoMYB46* promotes Pb²⁺ uptake, tolerance, and plant growth.

GRAPHICAL ABSTRACT
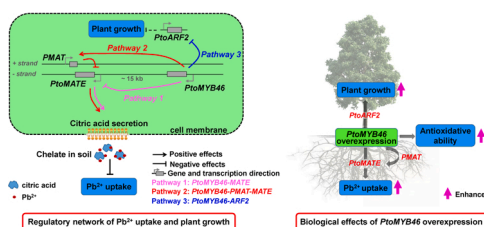
ARTICLE INFO

Editor: Dr. C. LingXin

ABSTRACT

Lead (Pb²⁺) is one of the most toxic heavy-metal contaminants. Fast-growing woody plants with substantial biomass are ideal for bioremediation. However, the transcriptional regulation of Pb²⁺ uptake in woody plants remains unclear. Here, we identified 226 Pb²⁺-induced, differentially expressed long non-coding RNAs (DELs) in *Populus tomentosa*. Functional annotation revealed that these DELs mainly regulate carbon metabolism, biosynthesis of secondary metabolites, energy metabolism, and signal transduction through their potential target genes. Association and epistasis analysis showed that the lncRNA *PMAT* (Pb²⁺-induced *multidrug and toxic compound extrusion* (*MATE*) antisense lncRNA) interacts epistatically with *PtoMYB46* to regulate leaf dry weight, photosynthesis rate, and transketolase activity. Genetic transformation and molecular assays showed that *PtoMYB46* reduces the expression of *PtoMATE* directly or indirectly through *PMAT*, thereby reducing the secretion of citric acid (CA) and ultimately promoting Pb²⁺ uptake. Meanwhile, *PtoMYB46* targets *auxin response factor 2* (*ARF2*) and reduces its expression, thus positively regulating plant growth. We concluded that the *PMAT–PtoMYB46–PtoMATE–PtoARF2* regulatory module control Pb²⁺ tolerance, uptake, and plant growth. This study demonstrates the involvement of lncRNAs in response to Pb²⁺ in poplar, yielding new insight into the potential for developing genetically improved woody plant varieties for phytoremediating lead-contaminated soils.

* Correspondence to: College of Biological Sciences and Technology, Beijing Forestry University, No. 35, Qinghua East Road, Beijing 100083, PR China.
  E-mail address: DeqiangZhang@bjfu.edu.cn (D. Zhang).

1. Introduction

Heavy-metal (HM) pollution is a growing environmental problem around the world, and lead (Pb^{2+}) is one of the most toxic heavy metal contaminants (Needleman, 2004) and a major pollutant in both terrestrial and aquatic ecosystems (Sharma and Dubey, 2005). Pb^{2+} is a strong reactant for protein N- and S- ligands and can cause the distortion of enzymes and structural proteins. Pb^{2+} can inhibit chlorophyll synthesis (Sengar and Pandey, 1996), electron transport (Rashid et al., 1994) and RubisCo activity (Stiborova et al., 1986) in the photosynthetic system. Pb^{2+} accumulation can stimulate the formation of free radicals and reactive oxygen species (ROS), leading to oxidative stress and damage to the cytoplasmic membrane (Jayalakshmi and Venkatachalam, 2011). Pb^{2+} also affects the nutritional status of plants, often limiting the uptake of essential elements such as calcium, magnesium and zinc (Gupta et al., 2013). A higher level of Pb^{2+} (80–240 mg·kg^{-1}) in soils can damage plant development, reduce survival, inhibit photosynthesis, and disturb plant nutrient and water balance (Saleem et al., 2018; Kumar and Kumari, 2015), which severely restrict the development of agriculture and forestry. Pb^{2+} in soil can easily be absorbed by plants and can eventually enter the food chain resulting in adverse consequences for human health, such as serious damage to the brain and central nervous system (El-Ansary et al., 2017; Wang et al., 2017a, 2017b). Therefore, it is imperative to remediate Pb^{2+}-contaminated soil.

Phytoremediation is an effective and low-cost strategy for the remediation of HM-contaminated soils. Many herbaceous plant species, such as *Sedum alfredii*, *Brassica juncea*, and *Pteris vittata* have remarkable abilities to accumulate HMs from the soil (Fayiga et al., 2004; Deng et al., 2007; Ueno et al., 2011). However, Pb^{2+} accumulation in these herbaceous plants is limited due to their shallow root systems and low biomass. Woody plants such as *Populus* species have been proposed as ideal candidates for phytoremediation due to their fast growth, accumulating huge biomass, and well-developed root systems (Luo et al., 2016). The main advantage of poplar for remediation of HM-contaminated soils is their huge biomass (Pulford and Watson, 2003), which results in a relatively high amount of Pb^{2+} extracted per plant (Di Lonardo et al., 2011) and yields large amounts of wood and biomass (González-Oreja et al., 2008). In soil containing 140 mg·kg^{-1} Pb^{2+}, maize and sunflower accumulated 88 μg and 176 μg Pb^{2+} per plant, respectively, whereas, poplar accumulated 629 μg Pb^{2+} per plant (Kacalkova et al., 2014), which demonstrate the great potential of poplars in the remediation of HM-contaminated soil. To further enhance the utility of poplars for Pb^{2+} remediation, it is crucial to obtain a better understanding of the physiological and transcriptional regulation mechanisms underlying poplar responses to Pb^{2+}.

The main mechanisms underlying plant responses to Pb^{2+} are changes in the uptake and transport pathways of Pb^{2+} and detoxification of cellular damage (Kumar and Prasad, 2018). Several genes have been identified in these crucial processes. For example, ABC transporters proteins such as ATM3 and PDR12 in *Arabidopsis thaliana* have been shown to be involved in mediating plant resistance to Pb^{2+} toxicity: transgenic lines overexpressing *ATM3* and *PDR12* had higher Pb^{2+} resistance and lower Pb^{2+} accumulation compared to wild-type plants (Kim et al., 2006; Lee et al., 2005). In *Arabidopsis*, rice, and mangroves, the expression of metallothionein synthesis-related genes is up-regulated under Pb^{2+} stress, improving their tolerance to Pb^{2+} (Xu et al., 2007; Kim and Kang, 2018). However, HM tolerance is a complex quantitative trait, and a single gene usually cannot fully explain the underlying mechanisms.

Long non-coding RNAs (lncRNAs) are key regulators of plant growth, development, and tolerance to various stresses (Song and Zhang, 2017; Kindgren et al., 2018; Cui et al., 2019). Recent studies have elucidated the regulatory roles of lncRNAs in ion uptake and transport in plants. In *Medicago truncatula*, the PHOSPHATE (Pi) DEFICIENCY-INDUCED lncRNA (*PDIL1*) suppresses the degradation of the *MtPHO2* mRNA by miR399, curtailing the degradation of Pi transporters, whereas the lncRNAs *PDIL2* and *PDIL3* negatively regulate the Pi transport gene *Mdetr1g074930* (Wang et al., 2017a, 2017b). In *Betula platyphylla*, cadmium (Cd) stress differentially regulates the expression of *LncRNA2705.1* and *LncRNA11415.1*, which in turn regulated their target genes, such as *LDHA* and *HSP18.1*, to increase Cd^{2+} stress tolerance (Wen et al., 2020). These findings provide insight into the complex regulation of plant tolerance to ionic and HM stress. Nevertheless, the regulatory networks of *Populus* lncRNAs for Pb^{2+} tolerance remain elusive.

To decipher the roles of lncRNAs in regulating Pb^{2+} tolerance in poplar, one-year-old *Populus tomentosa* clones ('1316') were exposed to short-term Pb^{2+} stress with 200 μM Pb^{2+}. Transcriptome and single-nucleotide polymorphism (SNP)-based association analyses were performed to construct regulatory networks involving Pb^{2+}-responsive lncRNAs and their potential target genes (PTGs). The potential expression regulation mechanisms were explored and verified by genetic transformation and molecular biology experiments. This study sheds light on the lncRNA-mediated genetic regulatory networks of poplar in response to Pb^{2+} stress and lays a foundation for genetic improvement to enhance the remediation of HM-contaminated soils by perennial woody plants.

2. Materials and methods

2.1. Plant materials and Pb^{2+} treatment

Multi-copies (ramets) of one-year-old *Populus tomentosa* clones ('1316') were planted in plastic pots (14 cm in diameter, 12 cm deep) containing fine soil matrix and cultivated in a greenhouse (day/night temperature, 26 °C/18 °C; relative humidity, 50–60%). For Pb^{2+} treatment, six seedlings with similar heights (ca. 30 cm) were divided into two groups (three seedlings each), then carefully washed and transferred to modified full-strength Hoagland nutrient solution (6 mM KNO_3, 4 mM $Ca(NO_3)_2 \cdot 4H_2O$, 2 mM $MgSO_4 \cdot 7H_2O$, 0.85 μM iron citrate, 46 μM H_3BO_3, 9 μM $MnCl_2 \cdot 4H_2O$, 0.76 μM $ZnSO_4 \cdot 7H_2O$, 0.32 μM $CuSO_4 \cdot 5H_2O$, and 0.11 μM $H_2MoO_4 \cdot 2H_2O$). $NH_4H_2PO_4$ was removed from Hoagland's solution to prevent precipitation of $Pb_3(PO_4)_2$ (Wierzbicka and Potocka, 2002). To determine the effect of Pb^{2+}, the nutrient solution was supplemented with 0 μM and 200 μM Pb(Ac)$_2$. Based on our preliminary experiments and other studies (Yu, 2011; Sárvári et al., 2002), 200 μM is a high concentration for short-term stress. The pH of the solution was adjusted to 6.0 ± 0.1 by adding 1 M HCl or NaOH solution.

2.2. Measurement of photosynthetic trait parameters

Following Pb^{2+} treatment, diurnal variation in photosynthesis was measured from 08:00–18:00 on a sunny day using the Li-6400 portable photosynthesis system (LI-COR, Lincoln, NE, USA). Four photosynthetic trait parameters were measured to estimate the effects of Pb^{2+} on plants: net photosynthetic rate (Pn), transpiration rate (Tr), stomatal conductance (Gs), and intercellular CO_2 concentration (Ci). Mature leaves from the same position of control and Pb^{2+}-treated plants were collected at 0 h (8:00), 2 h (10:00), 4 h (12:00), 6 h (14:00), 8 h (16:00), and 10 h (18:00) after treatment.

2.3. Identification of Pb-responsive lncRNAs and their PTGs

Fresh mature leaves from three control and three Pb^{2+}-treated plants at 6 h of treatment were harvested and immediately frozen in liquid nitrogen for RNA-sequencing (RNA-seq) (Supplementary Method S1). After data processing, clean reads were aligned to the *P. trichocarpa* reference genome (v3.0) using hisat2 software (https://ccb.jhu.edu/software/hisat2/). Reads with no more than three mismatches were assembled, filtered, and merged by cufflinks-2.2.1 (http://cole-trapnell-lab.github.io/cufflinks/manual/); the criteria used for filtering

were length > 200 nt, coverage exon $\geq$ 2, fragments per kilobase (kb) of transcript per million fragments (FPKM) $\geq$ 0.1 and class code: i, j, u, x, o. The coding potential of the resulting transcripts was predicted using the CPC/CNCI/CPAT/Pfam software, and the transcripts identified simultaneously using all four software were defined as lncRNA transcripts. StringTie (1.3.1) was used to calculate the FPKM values of both lncRNAs and coding genes. LncRNAs and mRNAs with |log$_2$fold change (FC)|$\geq$ 1 and false discovery rate (FDR) < 0.05 were considered Pb-responsive lncRNAs or genes.

Two methods were used to predict PTGs of lncRNAs depending on *cis*- or *trans*-acting regulatory effects. RefSeq genes located within + /− 10 kb from the transcriptional positions of lncRNAs were considered to be *cis* PTGs. The LncTar software was used to predict *trans* PTGs based on sequence complementarity and ΔG between lncRNA–mRNA pairs. All mRNAs with normalized free energy (ndG) $\leq$ −0.1 were predicted to be *trans* PTGs. To explore the potential roles of Pb-responsive lncRNAs, their differentially expressed PTGs were annotated using PopGenie (http://www.popgenie.org/) and Kyoto Encyclopedia of Genes and Genomes (KEGG) analysis (https://www.kegg.jp/blastkoala/).

2.4. Association analysis based on single and multiple SNPs

To dissect genotype-phenotype associations (GPAs), 435 unrelated individuals were phenotyped and genotyped, and a mixed linear model in Tassel v5.2 was used for GPA analysis (Bradbury et al., 2007) (Supplementary Method S2). Ten phenotypic traits (leaf area (LA), leaf dry weight (LDW), chlorophyll contents (Chl), physiological traits (Pn, Gs, and Tr), and chloroplast-related parameters (transketolase activity (TKT), ferredoxin proteins content (FDX), ferredoxin NADP$^+$ reductase activity (FNR), and rubisco activity (Ru)) were measured (Supplementary Method S2) and *P*-values $\leq$ 1/*n* (*n* representing the number of SNP markers) were set as the threshold for significant single SNP-based associations with pairwise kinship (K) and estimated membership probability (Q) to represent the effects of population relatedness and structure among individuals for the GPA analysis.

SNPs found to be significant in single SNP-trait associations at $P <$ 1.06 $\times$ 10^{-5} ($P <$ 1/*n*; a total of 94,030 SNPs) were analyzed for SNP–SNP pairwise interactions. Multifactor Dimensionality Reduction software (MDR, v3.0.2) was used to identify and characterize significant epistatic SNP markers (Hahn et al., 2003). The epistatic effects of each significant association pair were also estimated.

2.5. Gene isolation, vector construction, and plant transformation

PtoMYB46 cDNA was amplified using gene-specific primers (Table S1, S2) and cloned into a pBI121- enhanced green fluorescent protein (EGFP) vector for protein subcellular localization (Supplementary Method S3).

Furthermore, *PtoMYB46* cDNA was cloned into the pCXSN plant expression vector (Chen et al., 2009) at the *Xcm*I site under the control of the cauliflower mosaic virus (CaMV) 35 S promoter. The construct was mobilized into *Agrobacterium tumefaciens* strain GV3101, which was used for poplar transformation (Supplementary Method S4). The *Pto-MYB46* overexpression (OE) lines were confirmed by PCR, and three OE lines with high transcription levels were used for the determination of phenotype under Pb^{2+} treatment.

2.6. Analysis of transgenic poplar lines

Twenty-day old rooting plantlets of OE and wild-type(WT) lines were transferred to plastic pots containing fine soil matrix and cultivated in an artificial climate chamber. After 7 days of growth, OE and WT lines showing similar heights (ca. 12 cm) were selected for further analyses. The sixth to ninth leaves of 45-day-old WT and OE plants were used to assess several phenotypic traits, including Pn, Chl, TKT, LA, LDW, and plant height (H). After harvest, whole plants were washed with distilled

water and oven-dried at 105 °C for 24 h to determine whole-plant dry weight.

For Pb^{2+} treatment, the soil matrix was collected from the greenhouse of Beijing Forestry University, which contains 43.18 g·kg^{-1} organic matter, 82.18 g·kg^{-1} available N, 10.31 g·kg^{-1} available P, 169.78 g·kg^{-1} available K, and 19.1 g·kg^{-1} Pb^{2+}. After natural drying, the soil was ground and sieved through a 5-mm mesh. Pb(AC)$_2$ was then added to the soil meal to bring Pb^{2+} content in the soil to 600 mg·kg^{-1} and 10.0 kg homogeneous soils were incubated with 3 L water for one month, and the soils were always kept moist. WT and OE plants (45-day-old, 10 plants each line) of similar heights (ca. 35 cm) were planted in plastic pots (14 cm in diameter, 12 cm deep) with lead-incubated soil (600 mg·kg^{-1} Pb^{2+}, pH =6.82), whose parameters simulate the soil Pb^{2+} concentration and pH measured in the lead/zinc mining area of Liaocheng, Shandong province, China.

Three WT and OE plants were randomly selected before and after 20 days of the Pb^{2+} treatment. The whole plants were washed thoroughly with distilled water, and oven-dried at 105 °C for 25 h, after which their dry mass was determined. The growth rate of plant height and biomass were calculated as follows: growth rate = (data before treatment – data after treatment) / data after treatment × 100%. Dried mature leaves and roots (~100 mg) from WT and OE plants (three plants each line) after 20 days of Pb^{2+} treatment were powdered, sifted through 2-mm nylon screens, and digested in a mixture containing 7 mL concentrated HNO$_3$ and 1 mL concentrated HClO$_4$ at 170 °C. Pb^{2+}concentrations were determined by an inductively coupled plasma mass spectrometer (Agilent 7700x, Agilent Technologies, Santa Clara, CA, USA).

The activity of catalase (CAT) and malondialdehyde (MDA) content in leaves and citrate acid (CA) concentrations in root were detected using micro catalase assay kit (Solarbio® BC0205), micro malondialdehyde assay kit (Solarbio® BC0025), and citric acid content assay (Solarbio® BC2155), respectively, according to the manufacturers' instructions. Additionally, leaf and root samples were harvested from WT and OE plants for RNA isolation and quantitative reverse transcription-PCR (qRT-PCR) to detect the expression levels of *PMAT*, *PtoMYB46*, *PtoMATE*, and *PtoARF2* (gene-specific primers are listed in Table S2).

2.7. Molecular assays

To identify the target genes of the *PMAT-PtoMYB46* module and dissect their regulatory roles, a series of bioinformatics analyses and molecular experiments were performed, which include weighted gene correlation network analysis (WGCNA), DNA affinity purification sequencing (DAP-seq), dual-luciferase assays, yeast one-hybrid assays, and electrophoretic mobility shift assay (EMSA). All methods for these assays are described in Supplementary Method S5–S9.

2.8. Statistical analyses

All measurements in this study were carried out using at least three biological and three technical replicates. Statistical analyses were conducted using SPSS 22.0. Data are presented as mean ± standard deviation (SD).

3. Results

3.1. Time course of photosynthetic changes under Pb^{2+} stress

Photosynthetic changes of poplar (one-year-old) in response to Pb^{2+} stress were measured and compared to the control after 6 h (14:00) of Pb^{2+} treatment, Pn, Tr, and Gs levels were significantly reduced by 14.92%, 11.06%, and 22.08%, respectively, revealing that Pb^{2+} significantly inhibited leaf photosynthesis (Fig. 1A-C). After 8 h of Pb^{2+} exposure (16:00), the reductions in Pn, Tr, and Ci compared to control plants were accentuated. However, Ci increased significantly (24.82% higher than controls) (Fig. 1D), suggesting that the photosynthetic

system was damaged by Pb^{2+} treatment. This indicates that non-stomatal limitation had already become a major factor in Pb^{2+}-induced photosynthetic inhibition after 8 h of Pb^{2+} treatment. These results suggest that 6 h of Pb^{2+} exposure significantly inhibit photosynthesis, therefore samples after 6 h of Pb^{2+} exposure were used for subsequent studies.

3.2. Transcriptome analysis of Pb^{2+}-induced lncRNAs

3.2.1. Genome-wide identification of lncRNAs in P. tomentosa

To identify the lncRNAs involved in Pb^{2+} tolerance in *Populus*, transcriptome sequencing was performed using leaf samples from plants treated with Pb^{2+} for 6 h. In total, this identified 1171 expressed lncRNAs (FPKM$\geq$0.1 in at least one library), including 470 (40.1%) antisense lncRNAs, 330 (28.2%) sense lncRNAs, 272 (23.2%) intergenic lncRNAs, and 99 (8.5%) intronic RNAs. The lncRNAs ranged from 202 nt to 3127 nt, with an average of 423 nt, and were shorter than the protein-coding transcripts (average of 1705 nt) (Fig. S1A). The average expression levels of these lncRNAs were lower than those of the protein-coding transcripts (Fig. S1B). These lncRNAs were almost evenly distributed across the 19 chromosomes of the poplar genome (Fig. S1C). Notably, 56 lncRNAs were specifically expressed under Pb^{2+} stress (Table S3).

3.2.2. Pb^{2+}-induced lncRNAs and their PTGs

To identify Pb^{2+} responsive lncRNAs and protein-coding genes, the expression levels of all lncRNAs and mRNAs in the control and Pb^{2+} treatment groups were compared. There were 226 differentially expressed lncRNAs (DELs, $|\log_2(FC)| \geq 1$ and FDR < 0.05), including 81 up- and 145 down-regulated lncRNAs (Table S3). In addition, 5888 differentially expressed genes (DEGs, $|\log_2(FC)| \geq 1$ and FDR < 0.05) were detected, including 2454 up- and 3434 down-regulated DEGs (Table S4).

The PTGs of the 226 DELs were predicted based on the regulatory effects of lncRNAs on their targets (*cis* or *trans*-acting). In total, 4685 *cis*- and *trans*- PTGs were identified, corresponding to 7029 lncRNA–target pairs (LTPs), including 5159 *cis*- and 1870 *trans*-acting target pairs (Table S5, S6). Among these PTGs, 872 differentially expressed PTGs (DE-PTGs) were targeted by 214 DELs, corresponding to 1319 DE-lncRNA–target pairs (DE-LTPs), including 860 *cis*- and 459 *trans*-acting target pairs (Table S7). These DE-LTPs showed four different expression patterns: simultaneous up-regulation (Up-Up; 164 pairs), simultaneous down-regulation (Down-Down; 776 pairs), up-regulated lncRNA but down-regulated PTG (Up-Down; 145 pairs), and down-regulated lncRNA but up-regulated PTG (Down-Up; 234 pairs). These results indicate that these DELs regulate the expression of DE-PTGs via different interaction patterns.

To obtain more insights into the potential functions of DELs in the response to Pb^{2+} stress, their DE-PTGs were subjected to KEGG enrichment analysis. As a result, 206 of the 872 DE-PTGs were annotated to 69 different pathways. These included global and overview maps (carbon metabolism and biosynthesis of secondary metabolites), energy metabolism (photosynthesis, antenna proteins, carbon fixation in photosynthetic organisms, and sulfur metabolism), and signal transduction (MAPK signaling pathway, and plant hormone signal transduction) (Fig. S2, Table S8). We concluded that these DELs mainly respond to Pb^{2+} stress through these biological pathways.

3.2.3. Verification of RNA-seq data by qRT-PCR

To validate the reliability of the RNA-seq data, the expression patterns of eight DE-LTPs representing all four lncRNA–target expression patterns (Up-Up, Down-Down, Up-Down, and Down-Up) were detected by qRT-PCR. As shown in Fig. S1D, there was a significant positive correlation in the Pb^{2+}-induced changes in expression of each gene between the RNA-seq and qRT-PCR data ($R^2 = 0.92$), demonstrating the reliability of the sequencing data and confirming that these DE-LTPs
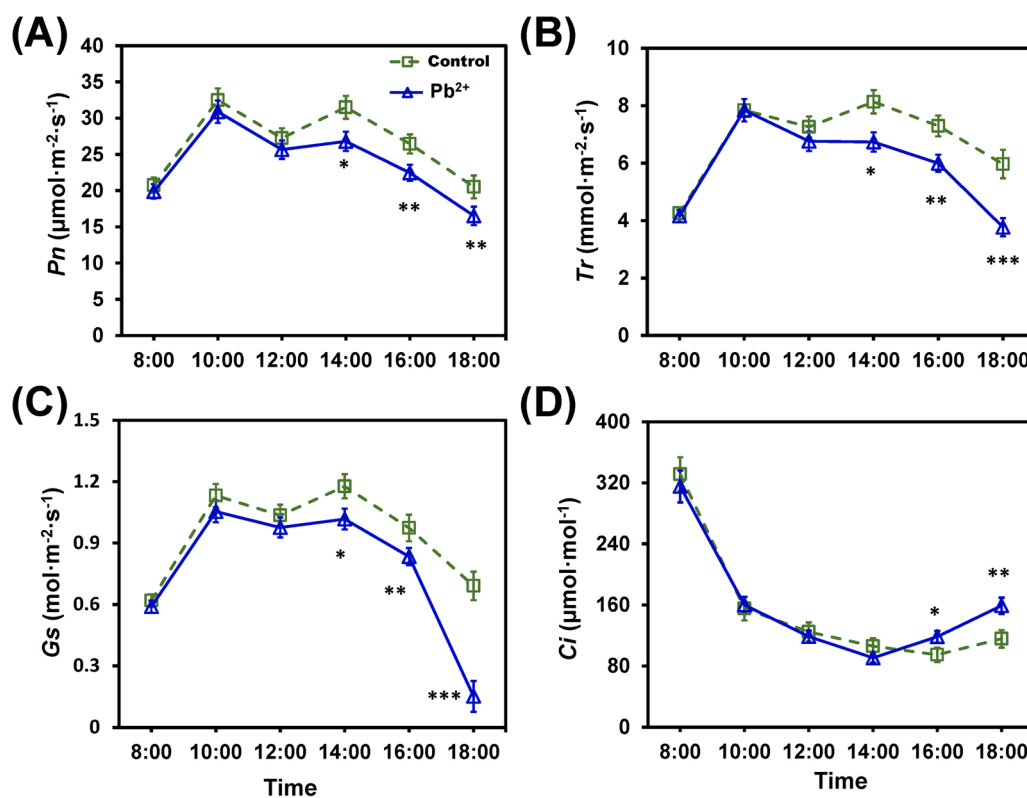

Fig. 1. Diurnal changes in photosynthetic traits of *P. tomentosa* in response to Pb^{2+} treatment. (A–D) Changes in the net photosynthetic rate (Pn), transpiration rate (Tr), stomatal conductance (Gs), and intercellular CO_2 concentration (Ci) at 0 (8:00), 2 (10:00), 4 (12:00), 6 (14:00), 8 (16:00), and 10 h (18:00) after Pb^{2+} treatment. Data are presented as means $\pm$ SD; (*$P < 0.05$, **$P < 0.01$, *** $P < 0.001$).

respond to Pb^{2+} treatment.

3.3. Genetic dissection of Pb^{2+}-induced lncRNAs and their PTGs

3.3.1. Analysis of single SNP-based associations

To further explore the effects of Pb^{2+}-induced DELs and DE-PTGs on phenotypic traits, single SNP-based associations were performed using a mixed linear model in TASSEL v5.2. Using the genomic resequencing data from 435 individuals, a total of 94,030 high-quality common SNPs (minor allele frequency >5%; missing data ≤10%) within 214 DEL genes and 872 DE-PTGs were identified. Association analysis identified 40 significant SNP–trait associations with *P*-values ≤ 1.06×10^{-5} (threshold = $1/n$), representing 36 unique SNPs associated with ten phenotypic traits (Table S9, S10; Fig. S3). These 36 SNPs were located in six DELs (16 SNPs) and seven DE-PTGs (20 SNPs). Each SNP explained 2.34–15.62% of the phenotypic variance (R^2); the most significant association was between PtoMYB46_SNP26 and LDW (*P*-value = 1.12×10^{-6}), which accounted for 13.50% of the variation (Table S10).

Among the 40 significant associations, 37 and 38 associations showed additive and dominance effects, respectively; 35 (87.5%) associations showed both additive and dominance effects (Table S10). At the genomic level, five DELs and six DE-PTGs showed significant associations with at least two phenotypic traits (Fig. 2A), and these pleiotropic genes had different effects on different phenotypic traits. For example, six pleiotropic genes (three DELs and three DE-PTGs) showed both additive and dominant effects while the five other pleiotropic genes (two

DELs and three DE-PTGs) showed mixed genetic effects on the phenotypic traits.

Four DE-LTPs were significantly associated with the same phenotypic traits, and their expression patterns under Pb^{2+} treatment are shown in Fig. 2A. For instance, both *PMAT* and *PtoMYB46* (homologous to *Arabidopsis* At*MYB46*) were significantly associated with LDW, Pn, and TKT activity. PMAT_SNP10, SNP11, and SNP15 were significantly associated with TKT, LDW, and Pn, respectively. All these loci are located in the 3′ untranslated region (UTR) of *PtoMATE* (the host gene of *PMAT*), and *PMAT* is located on the antisense strand from the last exon to the 3′ UTR of *PtoMATE*. MYB46_SNP24, SNP26, and SNP77 were significantly associated with TKT, LDW, and Pn, respectively (Fig. 2B, Table S10). These results suggest that these DELs may affect the physiology and leaf phenotypes of poplar under Pb^{2+} stress by regulating the expression of their target genes.

3.3.2. Epistasis analysis of DELs and DE-PTGs under Pb^{2+} stress reveals a complex genetic interaction network

Next, epistatic effects of the 36 significant SNPs between DE-LTPs across ten phenotypic traits were examined using the software MDR v3.0.2. Sixty-one significant epistatic pairs for ten traits were identified, representing epistatic interactions for phenotype traits among 24 unique SNPs, including 10 unique SNPs from six DELs and 14 unique SNPs from seven DE-PTGs (Table S11, S12). Among the 61 significant SNP interaction pairs, 27 and 6 showed epistatic interaction effects within DELs and DE-PTGs, respectively, and 28 showed epistatic interactions
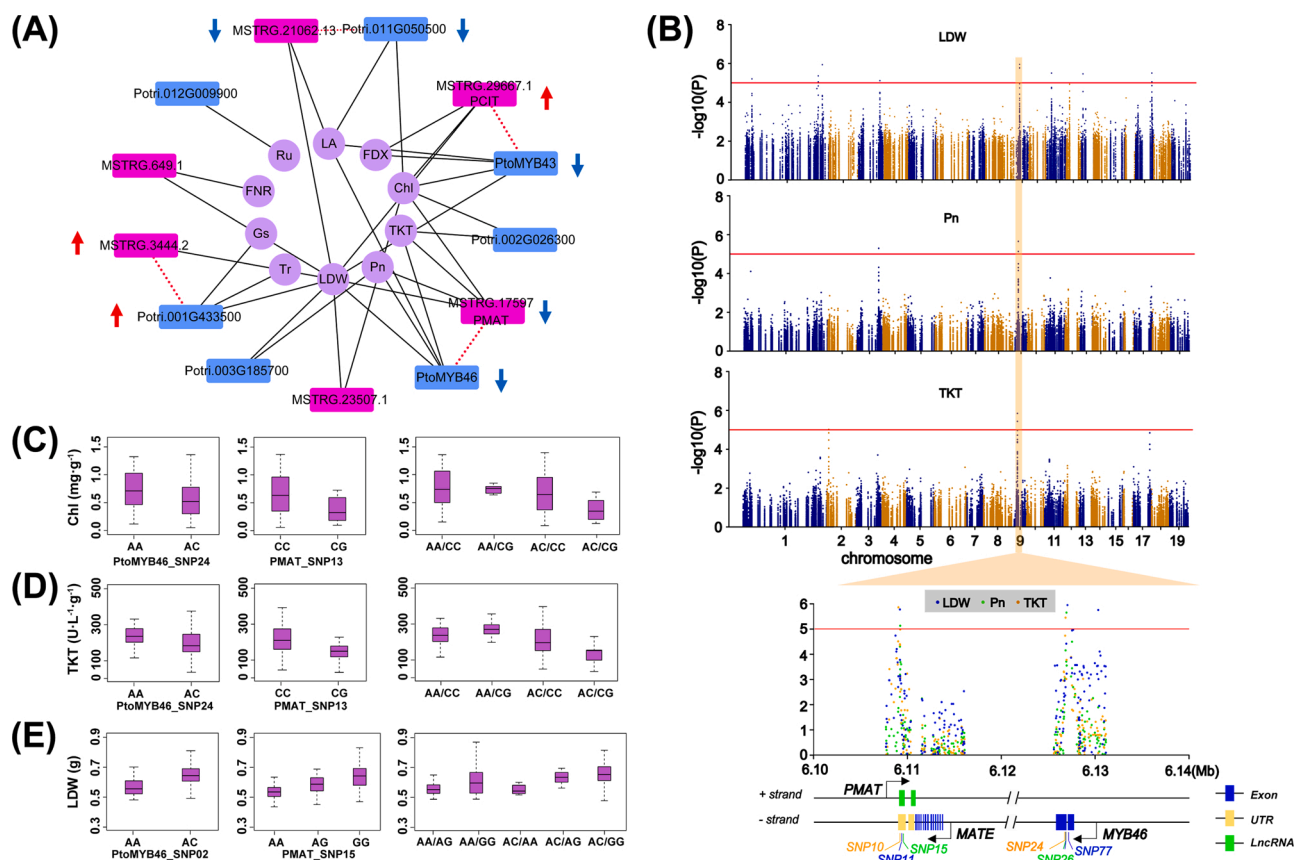

Fig. 2. Single SNP-based associations and epistatic effects of Pb^{2+}-responsive genes (DELs and their DE-PTGs) for 10 phenotypic traits in *P. tomentosa*. (A) Significant associations between Pb^{2+}-responsive genes (DELs and their DE-PTGs); magenta and blue rectangles represent DELs and DE-PTGs, respectively; purple circles represent the 10 phenotypic traits; red dotted lines represent DE-LTPs. Red arrows indicate up-regulation and blue arrows indicate down-regulation under Pb^{2+} treatment. (B) Significant associations of the *PMAT–PtoMYB46* target pair. (C–E) Single genotypic effects and pairwise effects of different genotype combinations on phenotypic traits: PtoMYB46_SNP24 and PMAT_SNP13 on chlorophyll content (C), PtoMYB46_SNP24 and PMAT_SNP13 on transketolase activity (D), and PtoMYB46_SNP02 and PMAT_SNP15 on leaf dry weight (E). Chl: chlorophyll contents, FDX: ferredoxin protein content, FNR: ferredoxin NADP$^+$ reductase activity, Gs: stomatal conductance, LA: leaf area, LDW: leaf dry weight, Pn: net photosynthetic rate, Ru: rubisco activity, TKT: transketolase activity, Tr: transpiration rate. (For interpretation of the references to colour in this figure, the reader is referred to the web version of this article.)

between DELs and DE-PTGs.

Two DE-LTPs showed epistatic interactions for multiple phenotypic traits (Table S11). For example, *PMAT* showed epistatic interactions with *PtoMYB46* for Chl, TKT, and LDW. These findings indicate that pairwise epistatic interactions had more substantial effects than single loci and that the different allele/genotype combinations had considerable effects on each trait. For the *PMAT–PtoMYB46* target pairs, the phenotypic values of Chl content and TKT varied across different genotypic combinations of PMAT_SNP24 and PtoMYB46_SNP13: average Chl content ranged from 0.34 mg·g^{-1} (AC/CG) to 0.70 mg·g^{-1} (AA/CG), and TKT ranged from 138.78 U·L^{-1}·g^{-1} (AC/CG) to 269.50 U·L^{-1}·g^{-1} (AA/CG) (Fig. 2C, 2D). In addition, LDW varied from 0.54 g (AC/AA) to 0.65 g (AC/GG) across different genotypic combinations of PMAT_SNP02 and PtoMYB46_SNP15 (Fig. 2E). These results provide strong evidence for interactions between DE-LTPs, especially *PtoMYB46* and *PMAT*, and the potential biological roles of these genes in poplar growth under Pb^{2+} stress.

3.4. *PtoMYB46* positively regulates poplar growth and Pb^{2+} uptake

To further verify the biological function of the *PMAT–PtoMYB46* module, the transcriptional regulatory function of *PtoMYB46* was first investigated. Sequence alignment of PtoMYB46 with its homologs in *Arabidopsis* (AtMYB46) showed that PtoMYB46 harbors the same two Myb_DNA-binding domains as AtMYB46 (Fig. S4A), suggesting that PtoMYB46 might play a regulatory role as a nuclear transcription factor (TF). The subcellular localization of PtoMYB46 was then examined. The

EGFP control was distributed in both the cytoplasm and nucleus, whereas PtoMYB46-EGFP preferentially localized to the nucleus (Fig. S4B), suggesting that PtoMYB46 is a nuclear TF.

To investigate the biological function of *PtoMYB46*, an overexpression vector was constructed and transformed into poplar. Among ten independent *PtoMYB46*-OE lines, three lines with the highest *PtoMYB46* expression levels were selected for further analysis (Fig. S5). As shown in Fig. 3A-B, after 45 days of normal growth, the average LA, LDW, Chl, H, TKT activity, and Pn, were significantly higher in OE lines than the WT, increasing by 64.8%, 57.3%, 6.4%, 36.5%, 48.1%, and 55.0%, respectively. To further study whether the overexpression of *PtoMYB46* in poplar affects Pb^{2+} uptake, 45-day-old WT and OE lines were exposed to 20 days of Pb^{2+} stress (Fig. 3C). The OE lines markedly exhibited higher growth rates in plant height and biomass, and CAT activity was significantly enhanced 72.0% while the MDA contents decreased 41.2% compared with WT (Fig. 3D). The OE lines had 192% and 162% times higher Pb^{2+} contents in roots and leaves than in WT plants, respectively (Fig. 3E). These results suggested that *PtoMYB46* positively regulates growth and enhances Pb^{2+} uptake.

3.5. *PtoMYB46* interacts with PMAT and its host gene PtoMATE

PMAT is an antisense lncRNA transcribed in the antisense strand of 3′ UTR of *PtoMATE* (Fig. 4A), which encodes a root citrate transporter and regulates aluminum tolerance. PtoMATE shares 72.39% amino acid sequence similarity with AtMATE and has the same nine transmembrane domains (Fig. S6, S7), suggesting that MATE is a transmembrane protein
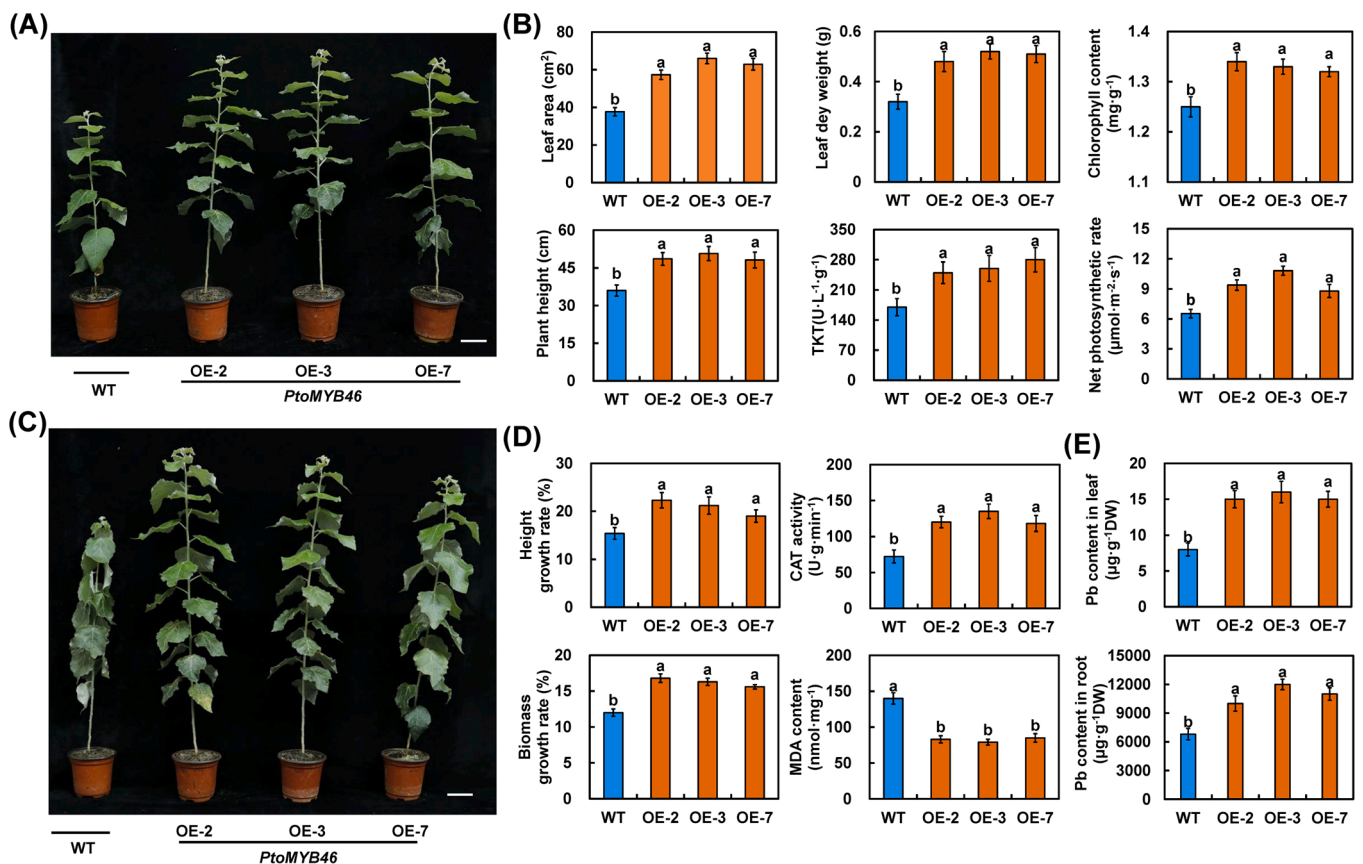

Fig. 3. *PtoMYB46* positively regulates poplar growth and Pb^{2+} tolerance. (A) Phenotypes of *PtoMYB46* overexpression and wild-type (WT) poplar lines under normal conditions. Scale bar 5 cm. (B) Leaf area (LA), leaf dry weight (LDW), chlorophyll content (Chl), plant height (H), transketolase activity (TKT), and net photosynthetic rate (Pn) of *PtoMYB46*-OE and WT plants. (C) Phenotypes of *PtoMYB46*-OE and WT lines after 20 days of further growth under 600 mg·kg^{-1} Pb^{2+} treatment. Scale bar 5 cm. (D) Height growth rate, biomass growth rate, catalase activity (CAT), and malondialdehyde contents (MDA) of *PtoMYB46*-OE and WT plants. (E) Pb^{2+} concentrations in the leaves and roots of *PtoMYB46*-OE and WT plants. Data are presented as means ± SD (*n* = 3). Bars with different lowercase letters indicate significant differences at *P* < 0.05.

with the same biological function as AtMATE. To determine whether PtoMATE acts as a target of the *PMAT–PtoMYB46* module and affects Pb^{2+} uptake, a DAP-seq assay of PtoMYB46 protein was performed. The most significantly enriched motif for PtoMYB46-binding was "ACCWAMY" (Fig. 4B, Fig. S8). The presence of potential PtoMYB46 binding sites in the *PtoMATE* promoter ('ACCAAAT', Table S2) and 3′ UTR (Fig. 4B, Table S2) suggests that PtoMYB46 might interact with the *PtoMATE* promoter and 3′ UTR, regulating the secretion of CA. To dissect their possible regulation pattern, a dual-luciferase assay was used to profile the effect of PtoMYB46 on *PtoMATE* and the *PMAT* transcript. The coding sequence of *PtoMYB46* and the full-length sequence of *PMAT* were amplified and cloned into pBI121 to act as effectors. The sequences of the *PtoMATE* promoter (*PtoMATEpro*), *PMAT*, 3′ UTR of *PtoMATE* (*MATE-3′ UTR*), and mutant *MATE-3′ UTR* (*MATE-3′ mUTR*) were amplified (Table S2) and cloned into pGreen-0800-Luc before and after the Luc coding sequence to act as reporters (Fig. 4C).

Overexpression of *PtoMYB46* repressed the fluorescence of *PtoMATEpro::Luc* and *35 S::Luc-MATE-3′ UTR* (Fig. 4D), indicating that PtoMYB46 not only inhibits the *MATE* promoter activity but also decreases *MATE* expression level by binding to its 3′ UTR. PtoMYB46

overexpression significantly enhanced the fluorescence of *35 S::Luc-PMAT*, while the expression of *35 S::PMAT* inhibited the fluorescence of *35 S::Luc-MATE-3′ UTR* (Fig. 4E), indicating that PtoMYB46 could indirectly inhibit *PtoMATE* expression by enhancing *PMAT* expression. Furthermore, *35 S::Luc-MATE-3′ UTR* co-transformed with *35 S::MYB46* and *35 S::PMAT* into *Nicotiana benthamiana* leaves resulted in significantly reduced fluorescence as compared to leaves that were co-transformed with *35 S::MYB46* and *35 S::Luc-MATE-3′ UTR* (Fig. 4F), revealing that *PMAT* expression increased the inhibitory effect of PtoMYB46 on *PtoMATE*. Further, the expression changes of *PMAT* and *PtoMATE* in *PtoMYB46*-OE poplars were determined, *PtoMYB46* overexpression increased the transcript abundance of PMAT and inhibited *MATE* transcription (Fig. 4G), which decreased CA secretion from the roots (Fig. 4H) and ultimately increased Pb^{2+} uptake.

3.6. PtoMYB46 directly targets and regulates the expression level of PtoARF2

To explore how the transcription network of *PtoMYB46* induces biomass production of poplar, WGCNA was used to detect potential
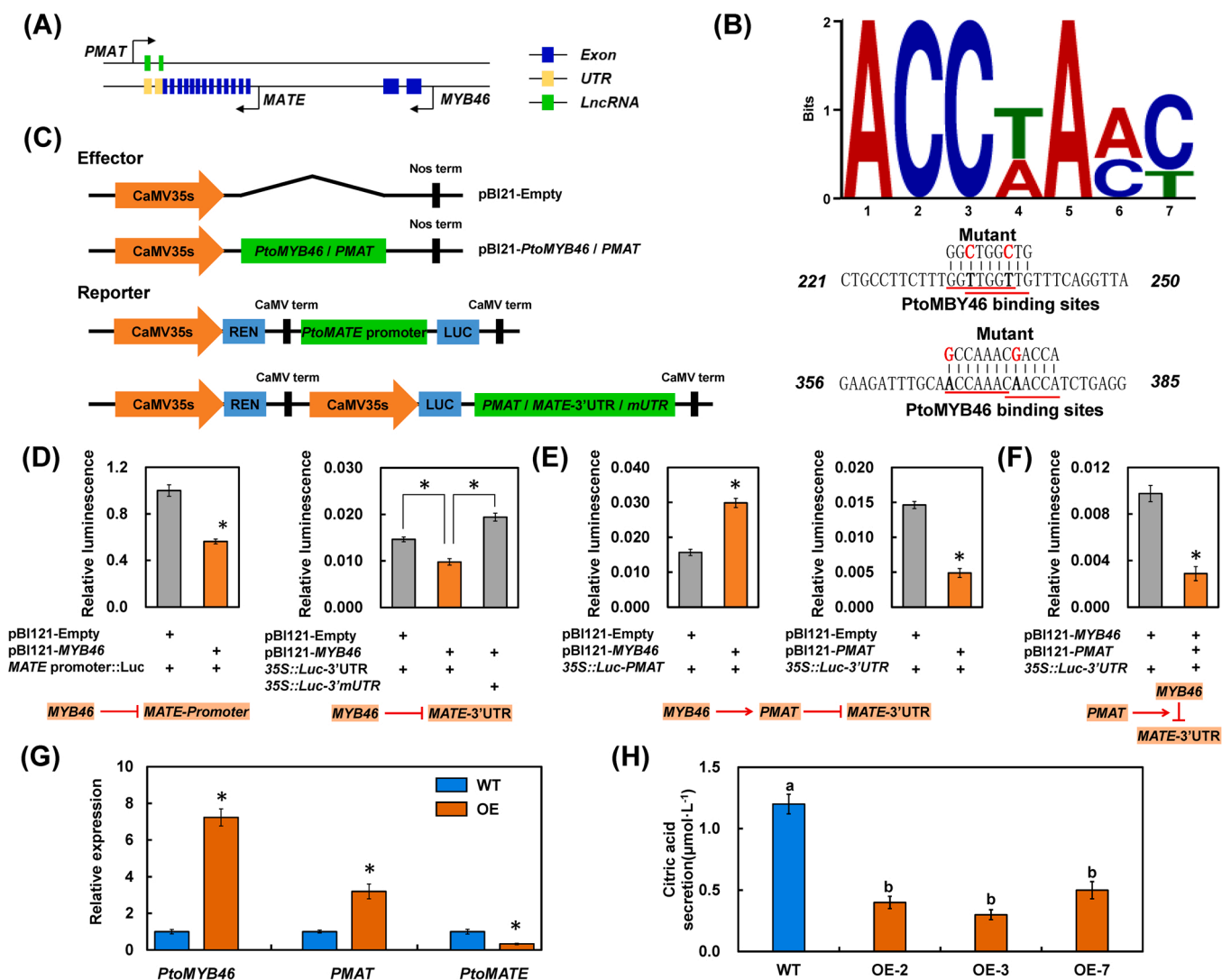

Fig. 4. PtoMYB46 targets *PMAT* and *PtoMATE*. (A) Schematic representation of the chromosomal locations of *PtoMYB46*, *PMAT*, and *PtoMATE*. (B) Sequence logo of the AtMYB46 binding motif and MYB46 target sequences within the 3′ UTR of *PtoMATE*. Four nucleotides were mutated in the 3′ UTR of *PtoMATE*. The numbers indicate the positions of the nucleotides in the reference wild-type sequences. (C) Schematic representation of the vectors used for the luciferase reporter assays. (D–F) The activity of the luciferase gene linked to the *PtoMATE* promoter or lncRNA *PMAT*, wild-type (*MATE* 3′ UTR), or mutant (mUTR) 3′ UTR of *PtoMATE*. (G) Relative expression of *PtoMYB46*, *PMAT,* and *PtoMATE* in *PtoMYB46*-OE lines under 600 mg·kg^{-1} Pb^{2+} treatment. (H) Citrate secretion from the root apices of *PtoMYB46*-OE and WT poplar plants under 600 mg·kg^{-1} Pb^{2+} treatment. Data are presented as means ± SD; (* $P < 0.05$).

interactions between DEGs (Fig. S9). Among 24 co-expressed modules, *PtoMYB46* was assigned to a module (blue) where AUXIN RESPONSE FACTOR2 (*PtoARF2*, homologous to *Arabidopsis AtARF2*, Fig. S10), a key regulator in cell division, plant growth, and senescence, showed the highest weighted value (0.493) with *PtoMYB46*, implying a possible interaction between *PtoMYB46* and *PtoARF2*. DAP-seq showed that the 'ACCAAAC' motif exists in the *PtoARF2* proximal promoter region (Fig. 5A, Table S2). A yeast one-hybrid assay and an EMSA assay indicated that *PtoMYB46* could directly bind to the *PtoARF2* promoter in vivo and in vitro, respectively (Fig. 5B, C). A dual-luciferase reporter assay showed that the *35 S::PtoMYB46* effector strongly inhibited the activity of the LUC reporter gene driven by the 1-kb promoter of *PtoARF2*, but this inhibition was abolished by mutations in the 'ACCAAAC' motifs in this promoter (Fig. 5D). In addition, *PtoMYB46* overexpression in transgenic poplars repressed *PtoARF2* transcript abundance (Fig. 5E). These results suggest that PtoMYB46 binds to the *PtoARF2* promoter directly and represses its expression. *PtoARF2*, a direct target of *PtoMYB46*, is involved in the regulation of poplar growth.

4. Discussion

4.1. Photosynthetic changes and lncRNA-mediated genetic regulation under Pb^{2+} stress

HMs have toxic effects on plants, impairing of plant growth and development, damaging the photosynthetic system, altering enzymatic activities, and causing oxidative injury (Clemens, 2001; Ding et al., 2017; Fahr et al., 2013). Among these metabolic processes, photosynthesis is one of the most stress-sensitive physiological traits (Paunov et al., 2018). In our study photosynthetic traits Pn, Tr, and Gs were significantly reduced after 6 h of Pb^{2+} treatment, indicating that short-term Pb^{2+} treatment significantly inhibits photosynthesis, perhaps

due to stomatal limitation. Pn, Tr, and Ci continued to decrease after 6 h of Pb^{2+} treatment, but Ci increased significantly, suggesting that the photosynthetic system was damaged by the Pb^{2+} treatment and that non-stomatal limitation was the major factor in Pb^{2+}-induced photosynthetic inhibition. This rapid inhibition and damage to photosynthesis indicated that poplar is sensitive to Pb^{2+} stress.

LncRNAs are known to have important roles in plant physiology and growth regulation (Tian et al., 2019; Zhang et al., 2019). In this study, 1319 DE-LTPs were identified in poplar under Pb^{2+} treatment. These DELs are primarily involved in carbon metabolism, biosynthesis of secondary metabolites, energy metabolism, and signal transduction pathways by regulating their DE-PTGs. SnRK2 kinases are core components of the ABA and osmotic stress signaling pathways (Lin et al., 2020) and the *snrk2* decuple mutant in *Arabidopsis* displays severe growth defects in soil and culture medium under osmotic stress conditions and greatly reduced responses to osmotic stress (Yan et al., 2017). *SnRK2* was down-regulated under Pb^{2+} treatment in poplar, indicating that ABA and osmotic stress signal transduction were weakened, perhaps at least partially explaining why plant growth was inhibited under Pb^{2+} treatment. *PtoSUR2* was annotated as having electron carrier and oxidoreductase activities, suggesting that the regulation of photosynthesis-related pathways might be repressed by Pb^{2+} stress, thereby reducing plant growth. Furthermore, mutations in *AtSUR2* leads to the overproduction of auxin in *Arabidopsis* (Maharjan et al., 2015), suggesting that *PtoSUR2* might modulate plant growth by affecting auxin biosynthesis. These findings together demonstrate that lncRNAs affect Pb^{2+}-responsive physiological processes by regulating energy metabolism, signal transduction, and phytohormone biosynthesis in poplar.

4.2. PtoMYB46 and PMAT modulate Pb^{2+} absorption in poplar

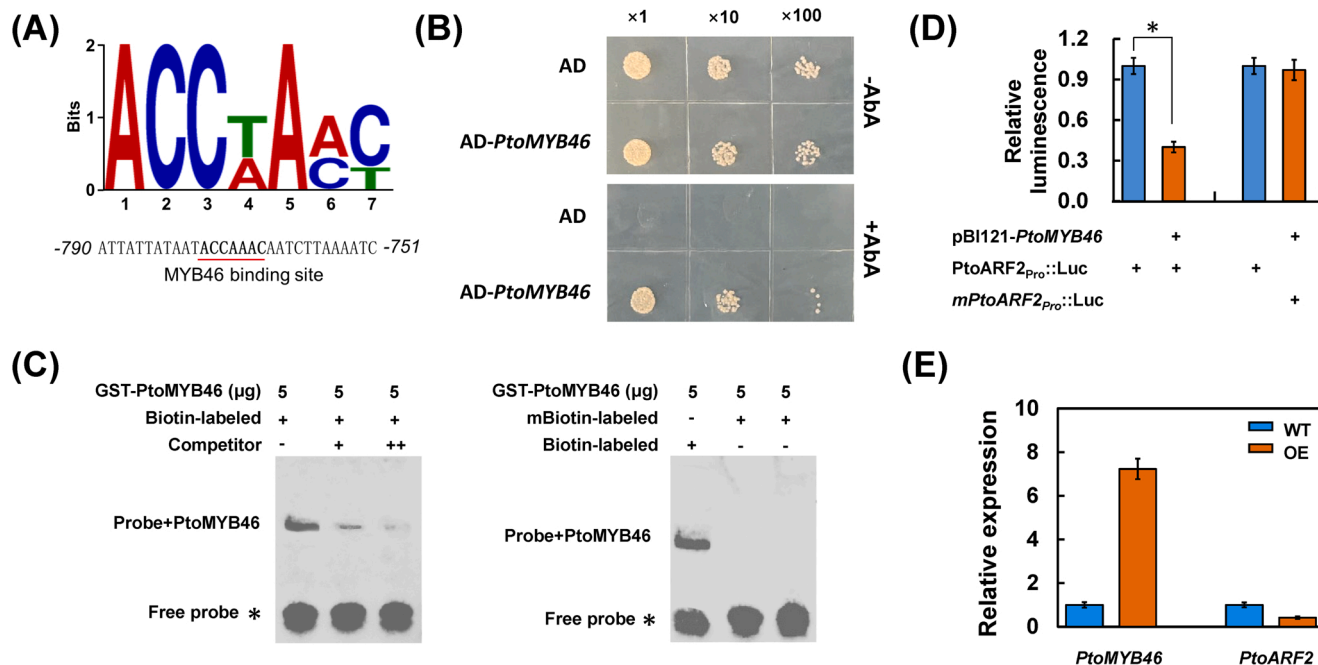Phytoremediation using trees is an emerging approach (Macek et al.,

Fig. 5. PtoMYB46 directly targets *PtoARF2*. (A) Sequence logo of the AtMYB46 binding motif and MYB46 target sequences within the promoter sequence of *PtoARF2*. The numbers indicate the positions of the nucleotides. (B) Physical interactions of PtoMYB46 with *PtoARF2* promoter in yeast one-hybrid assays. AD-*PtoMYB46* was introduced into *pAbAi-ARF2* Y1H Gold bait strain. The strains were grown on SD/–Leu medium either with or without aureobasidin A (AbA, 200 ng/mL) for 48–96 h at 30 °C. The empty vector *pGADT7* was employed as a negative control. (C) EMSA shows that the GST-PtoMYB46 recombinant protein binds to biotin-labeled probes of *PtoARF2*. Unlabeled probes were used as competitors. Mutant probes (Table S1) were labeled with biotin and used for EMSA with recombinant PtoMYB46. (D) Dual-luciferase assay of PtoARF2$_{Pro}$::LUC expression. The expression of REN was used as an internal control. The LUC/REN ratio represents the relative activity of the *PtoARF2* promoter. (E) Relative expression of *PtoMYB46* and *PtoARF2* in *PtoMYB46*-OE lines under 600 mg·kg^{-1} Pb^{2+} treatment. Data are presented as means ± SD; (*$P < 0.05$).

2000) and compared with herbs, the use of trees in the phytoremediation can produce a large amount of wood or biomass energy while achieving the remediation effect and realizing the resource utilization of polluted soil (González-Oreja et al., 2008). Possible end-product uses for woody plants include fuel for direct burning as wood chips, and raw material for the production of paper, chipboard and charcoal. (McElroy and Dawson, 1986; Yao et al., 2019), which can reduce the risk of HMs entering the food chain. In addition, HMs can be recovered by flue gas scrubbing and proper treatment of ash in biofuel applications of the woody plants (Perttu and Kowalik, 1997; Dahl, 2000), ultimately reducing the release of HMs. Therefore, woody plants have unique advantages for phytoremediation (Pulford and Watson, 2003). The efficiency of metal phytoextraction by woody plants depends on the multiplication of two factors: biomass yield × metal concentration in biomass (González-Oreja et al., 2008), suggesting a crucial role for the underlying genetic regulation of plant growth and phytoextraction capacity.

AtMATE is a citrate transporter found in *Arabidopsis* roots that confers Al^{3+} tolerance (Nakano et al., 2020). Overexpressing *PtrMATE1* increases the Al^{3+}-induced secretion of CA from the root apex in transgenic poplar. The Al^{3+}-induced inhibition of root growth is alleviated in both *Populus* and *Arabidopsis* when *PtrMATE1* is overexpressed (Li et al., 2017). These findings indicate that MATE proteins promote the transport and secretion of CA. The organic acid can chelate HMs to form non-toxic compounds that prevent them from entering plants (Yu et al., 2019). However, the effects of CA on Pb^{2+} accumulation by plants are inconsistent. In one study, CA significantly increased Pb^{2+} uptake by accumulating and non-accumulating *Sedum alfredii* plants (Lu et al., 2013). Conversely, CA treatment inhibited the uptake of Pb^{2+} or Cd^{2+} by radish (Chen et al., 2003), maize (Anwer et al., 2012), rice (Xue, 2020), and *Larix olgensis* (Song et al., 2018). Low concentrations of organic acids (exogenous oxalic acid (OA) and CA < 1.0 mmol·L^{-1}) reduced Pb^{2+} contents in fine roots and leaves may result from an external resistance mechanism, i.e., complexes of OA or CA and Pb^{2+} in soils inhibited Pb^{2+} adsorption into plants or soluble Pb^{2+} may be fixed on soil solid particles (Song et al., 2018). These results suggested that different mechanisms underlie the effects of CA on plant uptake of HMs. In our study, overexpression of *PtoMYB46* indirectly depressed the secretion of CA and promoted Pb^{2+} uptake by inhibiting *PtoMATE*. This inhibition effect is consistent with the results in radish, maize, rice, and *Larix olgensis*, and we deduce that the decrease in CA secretion weakens citrate chelation of Pb^{2+} and the inhibitory effect of CA on Pb^{2+} uptake, allowing Pb^{2+} to accumulate to higher levels in the transgenic lines.

3′ UTRs play important roles in the regulation of gene expression, as TFs interact with the 3′ UTRs of their target mRNAs. For example, the tumor-related TF Wilms' Tumor 1 preferentially binds to the 3′ UTRs of its development-related target genes, and this interaction antagonizes the binding of the degradation machinery directly or by stabilizing RNA structures (Bharathavikru et al., 2017). During the regulation of ethylene signal transduction in *Arabidopsis*, ETHYLENE INSENSITIVE 2 (EIN2) in the cytoplasm recognizes and binds to the 3′ UTR of *EIN3-BINDING F-BOX PROTEIN1/2* (*EBF1/2*) mRNA, and forms a P-body by recruiting relevant regulatory factors such as EIN5 and PABs, thereby inhibiting the translation of *EBF1/2* mRNA (Li et al., 2015; Merchante et al., 2015). In this study, PtoMYB46 not only inhibited the activity of the *MATE* promoter but also decreased the expression level of *MATE* by binding to its 3′ UTR. Therefore, we deduce that *PtoMYB46* not only inhibits the activity of the *MATE* promoter but also interacts with its 3′ UTR by directly binding or recruiting other proteins, reducing the mRNA stability of *PtoMATE*. For the *PtoMYB46–PMAT–MATE* pathway, *PtoMYB46* interacted with *PMAT* and enhanced its stability. TFs and lncRNA can recruit enzymes or TF protein to target and regulate their expression (Wang et al., 2015; Meredith et al., 2016; Xu et al., 2018). We deduce that *PtoMYB46* under the guidance of *PMAT*, or *PMAT* directly, binds or recruits other specific proteins, which act on the tail of *PtoMATE* (from the last exon to the 3′ UTR), inhibiting its transcription at the DNA

level and blocking the translation or reducing the stability of the *PtoMATE* mRNA at the RNA level.

Based on our results, two molecular pathways, *PtoMYB46–PtoMATE* and *PtoMYB46–PMAT–PtoMATE* (Fig. 6A), regulating Pb^{2+} uptake in poplar are proposed: *PtoMYB46* depresses the expression of *PtoMATE* directly or indirectly through *PMAT*, thereby reducing the secretion of CA and lead chelation in soil, and ultimately promoting Pb^{2+} uptake. The existence of *PMAT* in poplar increases the robustness of the *PtoMYB46–PtoMATE* regulatory module.

4.3. PtoMYB46 regulates plant growth in poplar under Pb^{2+} stress

Exposure to Pb^{2+} is highly toxic to plants. Symptoms of Pb^{2+} phytotoxicity include leaf chlorosis, reductions in photosynthesis, growth inhibition, and eventually decline of plant biomass (Jayalakshmi and Venkatachalam, 2011; Fahr et al., 2013; Gupta et al., 2013) which depress the efficiency of metal phytoextraction. Some types of stress-responsive TFs, such as MYB, WRKY, and HD-ZIP, trigger transcriptomic variations that are shared between physiological stress responses and growth regulation under stress treatment (Chen et al., 2017, 2019; Sharif et al., 2021). For example, plant MYBs regulate cell differentiation, organ formation, leaf morphogenesis, secondary metabolism, and abiotic stress responses (Ambawat et al., 2013; Qi et al., 2015; Sun et al., 2015; Ramírez et al., 2011). *BplMYB46* in *Betula platyphylla* not only improve salt tolerance and permeability by altering the expression of genes encoding key enzymes such as SOD, POD, and pyrroline-5-carboxylate synthase, thereby increasing reactive oxygen species scavenging and proline levels, but also regulate genes involved in secondary cell wall formation, increasing lignin deposition and secondary cell wall thickness (Guo et al., 2017). The lncRNA–target pair *MSTRG.22608.1–PtoMYB73* was induced by Cd^{2+} treatment in *P. tomentosa*, and the overexpression of *PtoMYB73* in *Arabidopsis* increased leaf biomass, photosynthetic rate, and Cd^{2+} contents in leaves (Quan et al., 2021). These studies demonstrate that key TFs have multiple genetic effects that can simultaneously regulate plant growth and acclimation to environmental stress and that their underlying mechanisms involve complex gene regulatory networks. In this study, *PtoMYB46* was induced by Pb^{2+} stress and was significantly downregulated. Association mapping revealed that *PtoMYB46* was simultaneously associated with LA, LDW, Pn, and TKT, pointing to the important role of *PtoMYB46* in regulating plant growth. Moreover, *PtoMYB46*-OE lines showed enhanced growth and Pb^{2+} tolerance. These results confirmed the notion that *PtoMYB46* enhances plant growth under normal conditions and in the presence of Pb^{2+} stresses.

In previous studies, the *arf2* mutants of *Arabidopsis* exhibited pleiotropic developmental phenotypes, including large, dark green rosette leaves; delayed flowering; thick and long inflorescence; large organ size; and delayed senescence and abscission (Ellis et al., 2005; Okushima et al., 2005). The seed size and weight of *arf2* mutant *Arabidopsis* increased significantly, caused by the extra cell division of the mutant's ovule, which led to seed coat expansion as ovule growth before fertilization determines the final seed size. The extra division of cells is due to the delay from the cell proliferation stage to the fully differentiated stage (Schruff et al., 2006; Hughes et al., 2008). It is suggested that *ARF2* is a general repressor of auxin-regulated cell division and organ growth (Schruff et al., 2006; Lim et al., 2010). In this study, PtoMYB46 directly binds to the *PtoARF2* promoter and represses its expression, indicating that *PtoMYB46* can positively regulate plant growth by targeting *PtoARF2*. Based on our results, we propose a model to explain how *PMAT* and *PtoMYB46* confer Pb^{2+} tolerance and regulate plant growth in poplar (Fig. 6A). Three molecular pathways regulate Pb^{2+} uptake and plant growth in poplar: (1) *PtoMYB46* directly represses the expression of *PtoMATE* by repressing its promoter activity and acting on its 3′ UTR. The down-regulation of *PtoMATE* reduces CA secretion and Pb^{2+} chelation in soil, ultimately increasing Pb^{2+} uptake. (2) *PtoMYB46* enhances the expression of lncRNA *PMAT*, and PMAT significantly decreases the
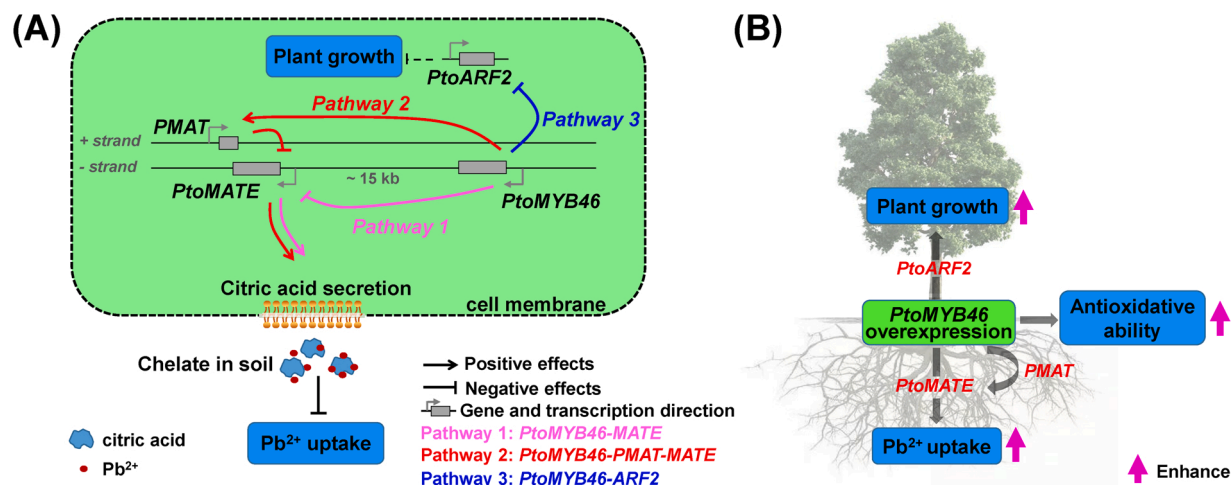
Fig. 6. Model of the regulatory network of Pb^{2+} uptake and plant growth involving *PMAT*, *PtoMYB46*, *PtoMATE*, and *PtoARF2* in *P. tomentosa* under Pb^{2+} treatment. (A) Regulatory network of Pb^{2+} uptake and plant growth. The black dashed lines represent plant growth regulatory pathways that needs further verification. The blue, red, and pink solid lines represent the Pb^{2+} uptake and plant growth regulatory pathways. The arrows denote positive effects, whereas lines ending with a short bar indicate negative effects. (B) Biological effects of *PtoMYB46* overexpression in *P. tomentosa*. Pink arrows indicate enhancement. (For interpretation of the references to colour in this figure, the reader is referred to the web version of this article.)

expression of *PtoMATE* by acting on the *MATE* 3′ UTR. In this pathway, PtoMYB46 indirectly inhibits the expression of *PtoMATE* and ultimately increases Pb^{2+} uptake. (3) PtoMYB46 targets *PtoARF2* and represses its expression, thereby positively regulating plant growth.

The ability of plants to uptake or accumulate HMs depends on a variety of factors, such as species specificity, plant growth characteristics (e.g., plant size, growth rate) and developmental stage, genetic regulation, HM concentrations in soil, rhizosphere pH and exposure time (Pietrini et al., 2010; Cheng et al., 2014; Shi et al., 2018; Fang et al., 2020). In this study, the parameters of the soil used to determine *PtoMYB46*-OE lines were simulated the soil Pb^{2+} concentration (600 mg·kg^{-1}) and pH (6.82) measured in the lead/zinc mining area of Liaocheng, Shandong province, China. However, the physical and chemical properties of Pb^{2+}-contaminated soils in different areas of China vary widely. For example, soil pH varies from 5.26 to 6.86 and Pb^{2+} concentration varies from 61.4 mg·kg^{-1} to 4090 mg·kg^{-1} in different lead–zinc mining areas in Huixian County, Northwest China (Zhan et al., 2014). Therefore, more different environmental factors should be taken into account in the determination of growth performance and Pb^{2+} tolerance of *PtoMYB46*-OE lines, including growth characteristics and developmental stage, Pb^{2+} concentration, soil pH, and exposure time. In conclusion, *PtoMYB46*-OE lines establish an excellent genetic regulation model for bioremediation (Fig. 6B) as the overexpression of *PtoMYB46* not only promotes lead absorption, but also increases antioxidant capacity and induces plant growth.

5. Conclusion

Using system biology approach, the present study provides a novel transcriptomic and genetic overview of the response of *Populus* to Pb^{2+} stress. Transcriptome analysis revealed that Pb^{2+}-induced DELs mainly regulate carbon metabolism, biosynthesis of secondary metabolites, energy metabolism, and signal transduction through their PTGs. Transcriptome analysis and association studies revealed that the target pair of *PtoMYB46* and the lncRNA *PMAT* is involved in regulating photosynthesis and growth traits in poplar under Pb^{2+} treatment. Overexpression of *PtoMYB46* in poplar promoted plant growth and enhanced Pb^{2+} tolerance and uptake. The subsequent molecular and biochemical assays showed that *PtoMYB46* depresses the expression of *PtoMATE* directly or indirectly through *PMAT*, thereby reducing the secretion of CA and ultimately promoting Pb^{2+} uptake. Meanwhile, *PtoMYB46* directly targeted *PtoARF2* and positively regulated plant growth.

Furthermore, transgenic poplar lines provide an excellent bioremediation model system where the overexpression of *PtoMYB46* not only promote Pb^{2+} uptake but also increase antioxidant capacity and promote plant growth.

CRediT authorship contribution statement

Panfei Chen: Investigation, Methods, Writing – original draft. **Yuepeng Song:** Writing – original draft. **Xin Liu:** Investigation, Methods. **Liang Xiao:** Software, Methods. **Chenhao Bu:** Software, Formal analysis. **Peng Liu:** Software, Formal analysis. **Lei Zhao:** Methods, Validation. **Pär Ingvarsson:** Writing – review & editing. **Harry Wu:** Writing – review & editing. **Yousry A. El-Kassaby:** Writing – review & editing. **Deqiang Zhang:** Conceptualization, Project administration, Supervision, Funding acquisition, Writing – review & editing.

Accession numbers

All transcriptome expression data have been deposited in the Genome Sequence Archive in the BIG Data Center (BIG, CAS, China) under accession number CRA003647 (https://bigd.big.ac.cn/).

Declaration of Competing Interest

The authors declare that they have no known competing financial interests or personal relationships that could have appeared to influence the work reported in this paper.

Appendix A. Supporting information

Supplementary data associated with this article can be found in the online version at doi:10.1016/j.jhazmat.2022.128769.

References

Ambawat, S., Sharma, P., Yadav, N.R., Yadav, R.C., 2013. MYB transcription factor genes as regulators for plant responses: an overview. Physiol. Mol. Biol. Plants 19, 307–321.

Anwer, S., Ashraf, M.Y., Hussain, M., Ashraf, M.Y., Jamil, A., 2012. Citric acid mediated phytoextraction of cadmium by maize (*Zea mays* L.). Pak. J. Bot. 44, 1831–1836.

Bharathavikru, R., Dudnakova, T., Aitken, S., Slight, J., Artibani, M., Hohenstein, P., Tollervey, D., Hastie, N., 2017. Transcription factor Wilms' tumor 1 regulates developmental RNAs through 3′ UTR interaction. Gene. Dev. 31, 347–352.

Bradbury, P.J., Zhang, Z., Kroon, D.E., Casstevens, T.M., Ramdoss, Y., Buckler, E.S., 2007. TASSEL: software for association mapping of complex traits in diverse samples. Bioinformatics 23, 2633–2635.

Chen, J., Nolan, T.M., Ye, H., Zhang, M., Tong, H., Xin, P., Chu, J., Chu, C., Li, Z., Yin, Y., 2017. *Arabidopsis WRKY46*, *WRKY54*, and *WRKY70* transcription factors are involved in brassinosteroid-regulated plant growth and drought responses. Plant Cell 29, 1425–1439.

Chen, S., Songkumarn, P., Liu, J., Wang, G.L., 2009. A versatile zero background T-vector system for gene cloning and functional genomics. Plant Physiol. 150, 1111–1121.

Chen, Y.S., Ho, T.D., Liu, L., Lee, D.H., Lee, C.H., Chen, Y.R., Lin, S.Y., Lu, C.A., Yu, S.M., 2019. Sugar starvation-regulated MYBS2 and 14-3-3 protein interactions enhance plant growth, stress tolerance, and grain weight in rice. Proc. Natl. Acad. Sci. U. S. A 116, 21925–21935.

Chen, Y.X., Lin, Q., Luo, Y.M., He, Y.F., Zhen, S.J., Yu, Y.L., Tian, G.M., Wong, M.H., 2003. The role of citric acid on the phytoremediation of heavy metal contaminated soil. Chemosphere 50, 807–811.

Cheng, H., Jiang, Z.Y., Liu, Y., Ye, Z.H., Wu, M.L., 2014. Metal (Pb, Zn and Cu) uptake and tolerance by mangroves in relation to root anatomy and lignification/suberization. Tree Physiol. 34, 646–656.

Clemens, S., 2001. Molecular mechanisms of plant metal tolerance and homeostasis. Planta 212, 475–486.

Cui, J., Jiang, N., Meng, J., Yang, G., Liu, W., Zhou, X., Ma, N., Hou, X., Luan, Y., 2019. LncRNA33732-respiratory burst oxidase module associated with WRKY1 in tomato-*Phytophthora infestans* interactions. Plant J. 97, 933–946.

Dahl, J., 2000. Chemistry and behavior of environmentally relevant heavy metals in biomass combustion and thermal ash treatment processes (Ph.D. thesis). Technical University of Graz,, Austria.

Deng, J., Liao, B., Ye, M., Deng, D., Lan, C., Shu, W., 2007. The effects of heavy metal pollution on genetic diversity in zinc/cadmium hyperaccumulator *Sedum alfredii* populations. Plant Soil 297, 83–92.

Di Lonardo, S., Capuana, M., Arnetoli, M., Gabbrielli, R., Gonnelli, C., 2011. Exploring the metal phytoremediation potential of three *Populus alba* L. clones using an in vitro screening. Environ. Sci. Pollut. Res. 18, 82–90.

Ding, S., Ma, C., Shi, W., Liu, W., Lu, Y., Liu, Q., Luo, Z.B., 2017. Exogenous glutathione enhances cadmium accumulation and alleviates its toxicity in *Populus × canescens*. Tree Physiol. 37, 1697–1712.

El-Ansary, A., Bjørklund, G., Tinkov, A.A., Skalny, A.V., Al Dera, H., 2017. Relationship between selenium, lead, and mercury in red blood cells of Saudi autistic children. Metab. Brain Dis. 32, 1073–1080.

Ellis, C.M., Nagpal, P., Young, J.C., Hagen, G., Guilfoyle, T.J., Reed, J.W., 2005. AUXIN RESPONSE FACTOR1 and AUXIN RESPONSE FACTOR2 regulate senescence and floral organ abscission in *Arabidopsis thaliana*. Development 132, 4563–4574.

Fahr, M., Laplaze, L., Bendaou, N., Hocher, V., El Mzibri, M., Bogusz, D., Smouni, A., 2013. Effect of lead on root growth. Front. Plant Sci. 4, 175.

Fang, Q., Zhang, J., Zhang, Y., Fan, N., van den Burg, H.A., Huang, C.F., 2020. Regulation of aluminum resistance in *Arabidopsis* involves the SUMOylation of the zinc finger transcription factor STOP1. Plant Cell 32, 3921–3938.

Fayiga, A.O., Ma, L.Q., Cao, X.D., Rathinasabapathi, B., 2004. Effects of heavy metals on growth and arsenic accumulation in the arsenic hyperaccumulator *Pteris vittata* L. Environ. Pollut. 132, 289–296.

González-Oreja, J.A., Rozas, M.A., Alkorta, I., Garbisu, C., 2008. Dendroremediation of heavy metal polluted soils. Rev. Environ. Health 23, 223–234.

Guo, H., Wang, Y., Wang, L., Hu, P., Wang, Y., Jia, Y., Zhang, C., Zhang, Y., Zhang, Y., Wang, C., Yang, C., 2017. Expression of the MYB transcription factor gene *BplMYB46* affects abiotic stress tolerance and secondary cell wall deposition in *Betula platyphylla*. Plant Biotechnol. J. 15, 107–121.

Gupta, D.K., Huang, H.G., Corpas, F.J., 2013. Lead tolerance in plants: strategies for phytoremediation. Environ. Sci. Pollut. Res. Int. 20, 2150–2161.

Hahn, L.W., Ritchie, M.D., Moore, J.H., 2003. Multifactor dimensionality reduction software for detecting gene-gene and gene-environment interactions. Bioinformatics 19, 376–382.

Hughes, R., Spielman, M., Schruff, M.C., Larson, T.R., Graham, I.A., Scott, R.J., 2008. Yield assessment of integument-led seed growth following targeted repair of auxin response factor 2. Plant Biotechnol. J. 6, 758–769.

Jayalakshmi, N., Venkatachalam, P., 2011. Biochemical and molecular effects of lead heavy metal toxicity in plants: a phytoremediation approach. Plant Cell Biotechnol. Mol. Biol. 12, 1–14.

Kacalkova, L., Tlustos, P., Szakova, J., 2014. Chromium, nickel, cadmium, and lead accumulation in maize, sunflower, willow, and poplar. Pol. J. Environ. Stud. 23, 753–761.

Kim, D.Y., Bovet, L., Kushnir, S., Noh, E.W., Martinoia, E., Lee, Y., 2006. *AtATM3* is involved in heavy metal resistance in *Arabidopsis*. Plant Physiol. 140, 922–932.

Kim, Y.O., Kang, H., 2018. Comparative expression analysis of genes encoding metallothioneins in response to heavy metals and abiotic stresses in rice (*Oryza sativa*) and *Arabidopsis thaliana*. Biosci. Biotechnol. Biochem 82, 1656–1665.

Kindgren, P., Ard, R., Ivanov, M., Marquardt, S., 2018. Transcriptional read-through of the long non-coding RNA SVALKA governs plant cold acclimation. Nat. Commun. 9, 4561.

Kumar, A., Prasad, M.N.V., 2018. Plant-lead interactions: Transport, toxicity, tolerance, and detoxification mechanisms. Ecotoxicol. Environ. Saf. 166, 401–418.

Kumar, G.H., Kumari, J.P., 2015. Heavy metal lead influative toxicity and its assessment in phytoremediating plants—a review. Water Air Soil Pollut. 226, 324.

Lee, M., Lee, K., Lee, J., Noh, E.W., Lee, Y., 2005. *AtPDR12* contributes to lead resistance in *Arabidopsis*. Plant Physiol. 138, 827–836.

Li, N., Meng, H., Xing, H., Liang, L., Zhao, X., Luo, K., 2017. Genome-wide analysis of MATE transporters and molecular characterization of aluminum resistance in *Populus*. J. Exp. Bot. 68, 5669–5683.

Li, W., Ma, M., Feng, Y., Li, H., Wang, Y., Ma, Y., Li, M., An, F., Guo, H., 2015. EIN2-directed translational regulation of ethylene signaling in *Arabidopsis*. Cell 163, 670–683.

Lim, P.O., Lee, I.C., Kim, J., Kim, H.J., Ryu, J.S., Woo, H.R., Nam, H.G., 2010. Auxin response factor 2 (ARF2) plays a major role in regulating auxin-mediated leaf longevity. J. Exp. Bot. 61, 1419–1430.

Lin, Z., Li, Y., Zhang, Z., Liu, X., Hsu, C.C., Du, Y., Sang, T., Zhu, C., Wang, Y., Satheesh, V., Pratibha, P., Zhao, Y., Song, C.P., Tao, W.A., Zhu, J.K., Wang, P., 2020. A RAF-SnRK2 kinase cascade mediates early osmotic stress signaling in higher plants. Nat. Commun. 11, 613.

Lu, L.L., TIAN, S.K., YANG, X.E., PENG, H.Y., LI, T.Q., 2013. Improved cadmium uptake and accumulation in the hyperaccumulator *Sedum alfredii*: the impact of citric acid and tartaric acid. J. Zhejiang Univ. -Sci. B 14, 106–114.

Luo, Z.B., He, J., Polle, A., Rennenberg, H., 2016. Heavy metal accumulation and signal transduction in herbaceous and woody plants: paving the way for enhancing phytoremediation efficiency. Biotechnol. Adv. 34, 1131–1148.

Macek, T., Mackova, M., Ka, J., 2000. Exploitation of plants for the removal of organics in environmental remediation. Biotechnol. Adv. 18, 23–34.

Maharjan, P.M., Dilkes, B.P., Fujioka, S., Pěnčík, A., Ljung, K., Burow, M., Halkier, B.A., Choe, S., 2015. *Arabidopsis* gulliver1/superroot2-7 identifies a metabolic basis for auxin and brassinosteroid synergy. Plant J. 80, 797–808.

McElroy, G.H., Dawson, W.M., 1986. Biomass from short-rotation coppice willow on marginal land. Biomass 10, 225–240.

Merchante, C., Brumos, J., Yun, J., Hu, Q., Spencer, K.R., Enríquez, P., Binder, B.M., Heber, S., Stepanova, A.N., Alonso, J.M., 2015. Gene-specific translation regulation mediated by the hormone-signaling molecule EIN2. Cell 163, 684–697.

Meredith, E.K., Balas, M.M., Sindy, K., Haislop, K., Johnson, A.M., 2016. An RNA matchmaker protein regulates the activity of the long noncoding RNA HOTAIR. RNA 22, 995–1010.

Nakano, Y., Kusunoki, K., Maruyama, H., Enomoto, T., Tokizawa, M., Iuchi, S., Kobayashi, M., Kochian, L.V., Koyama, H., Kobayashi, Y., 2020. A single-population GWAS identified *AtMATE* expression level polymorphism caused by promoter variants is associated with variation in aluminum tolerance in a local *Arabidopsis* population. Plant Direct 4, e00250.

Needleman, H., 2004. Lead poisoning. Annu. Rev. Med. 55, 209–222.

Okushima, Y., Mitina, I., Quach, H.L., Theologis, A., 2005. AUXIN RESPONSE FACTOR 2 (*ARF2*): a pleiotropic developmental regulator. Plant J. 43, 29–46.

Paunov, M., Koleva, L., Vassilev, A., Vangronsveld, J., Goltsev, V., 2018. Effects of different metals on photosynthesis: cadmium and zinc affect chlorophyll fluorescence in Durum Wheat. Int. J. Mol. Sci. 19, 787.

Perttu, K.L., Kowalik, P.J., 1997. Salix vegetation filters for purification of waters and soils. Biomass Bioenergy 12, 9–19.

Pietrini, F., Zacchini, M., Iori, V., Pietrosanti, L., Bianconi, D., Massacci, A., 2010. Screening of poplar clones for cadmium phytoremediation using photosynthesis, biomass and cadmium content analyses. Int. J. Phytoremediat. 12, 105–120.

Pulford, I.D., Watson, C., 2003. Phytoremediation of heavy metal-contaminated land by trees—a review. Environ. Int. 29, 529–540.

Qi, T., Huang, H., Song, S., Xie, D., 2015. Regulation of jasmonate-mediated stamen development and seed production by a bHLH-MYB complex in *Arabidopsis*. Plant Cell 27, 1620–1633.

Quan, M.Y., Liu, X., Xiao, L., Chen, P.F., Song, F.Y., Lu, W.J., Song, Y.P., Zhang, D.Q., 2021. Transcriptome analysis and association mapping reveal the genetic regulatory network response to cadmium stress in *Populus tomentosa*. J. Exp. Bot. 72, 576–591.

Ramírez, V., Agorio, A., Coego, A., García-Andrade, J., Hernández, M.J., Balaguer, B., Ouwerkerk, P.B., Zarra, I., Vera, P., 2011. MYB46 modulates disease susceptibility to *Botrytis cinerea* in *Arabidopsis*. Plant Physiol. 155, 1920–1935.

Rashid, A., Camm, E.L., Ekramoddoullah, A.K.M., 1994. Molecular mechanism of action of Pb^{2+} and Zn^{2+} on water oxidizing complex of photosystem II. FEBS Lett. 350, 296–298.

Saleem, M., Ahmad, Z., Shahid, M., 2018. Impact of lead tolerant plant growth promoting rhizobacteria on growth, physiology, antioxidant activities, yield and lead content in sun flower in lead contaminated soil. Chemosphere 195, 606e614.

Sárvári, É., Gáspár, L., Fodor, F., Cseh, E., Kröpfl, K., Varga, A., Baron, M., 2002. Comparison of the effects of Pb treatment on thylakoid development in poplar and cucumber plants. Acta Biol. Szeged. 46, 163–165.

Sengar, R.S., Pandey, M., 1996. Inhibition of chlorophyll biosynthesis by lead in greening *Pisum sativum* leaf segments. Biol. Plant. 38, 459–462.

Schruff, M.C., Spielman, M., Tiwari, S., Adams, S., Fenby, N., Scott, R.J., 2006. The *AUXIN RESPONSE FACTOR 2* gene of *Arabidopsis* links auxin signaling, cell division, and the size of seeds and other organs. Development 133, 251–261.

Sharif, R., Raza, A., Chen, P., Li, Y., El-Ballat, E.M., Rauf, A., Hano, C., El-Esawi, M.A., 2021. HD-ZIP gene family: Potential roles in improving plant growth and regulating stress-responsive mechanisms in plants. Genes 12, 1256.

Sharma, P., Dubey, R.S., 2005. Lead toxicity in plants. Braz. J. Plant Physiol. 17, 35–52.

Shi, W., Zhang, Y., Chen, S., Polle, A., Rennenberg, H., Luo, Z.B., 2018. Physiological and molecular mechanisms of heavy metal accumulation in nonmycorrhizal versus mycorrhizal plants. Plant Cell Environ. 42, 1087–1103.

Song, J.F., Markewitz, D., Wu, S., Sang, Y., Duan, C., Cui, X.Y., 2018. Exogenous oxalic acid and citric acid improve lead (Pb) tolerance of *Larix olgensis* A. Henry seedlings. Forests 9, 510.

Song, Y., Zhang, D., 2017. The role of long noncoding RNAs in plant stress tolerance. Methods Mol. Boil 1631, 41–68.

Stiborova, M., Doubravova, M., Leblova, S., 1986. Comparative study of the effect of heavy metal ions on ribulose-1,5-bisphosphate carboxylase and phosphoenolpyruvate carboxylase. Bichem. Physiol. Pflanz. 181, 373–379.

Sun, X., Gong, S.Y., Nie, X.Y., Li, Y., Li, W., Huang, G.Q., Li, X.B., 2015. A R2R3-MYB transcription factor that is specifically expressed in cotton (*Gossypium hirsutum*) fibers affects secondary cell wall biosynthesis and deposition in transgenic *Arabidopsis*. Physiol. Plant 154, 420–432.

Tian, Y., Zheng, H., Zhang, F., Wang, S., Ji, X., Xu, C., He, Y., Ding, Y., 2019. PRC2 recruitment and H3K27me3 deposition at *FLC* require FCA binding of *COOLAIR*. Sci. Adv. 5, eaau7 246..

Ueno, D., Milner, M.J., Yamaji, N., Yokosho, K., Koyama, E., Zambrano, M.C., Kaskie, M., Ebbs, S., Kochian, L.V., Ma, J.F., 2011. Elevated expression of *TcHMA3* plays a key role in the extreme Cd tolerance in a Cd-hyperaccumulating ecotype of Thlaspi caerulescens. Plant J. 66, 852–862.

Wang, S., Wu, W., Liu, F., Liao, R., Hu, Y., 2017a. Accumulation of heavy metals in soil-crop systems: a review for wheat and corn. Environ. Sci. Pollut. Res. Int. 24, 15209–15225.

Wang, T., Zhao, M., Zhang, X., Liu, M., Yang, C., Chen, Y., Chen, R., Wen, J., Mysore, K. S., Zhang, W.H., 2017b. Novel phosphate deficiency-responsive long non-coding RNAs in the legume model plant *Medicago truncatula*. J. Exp. Bot. 68, 5937–5948.

Wang, Y., He, L., Du, Y., Zhu, P., Huang, G., Luo, J., Yan, X., Ye, B., Li, C., Xia, P., Zhang, G., Tian, Y., Chen, R., Fan, Z., 2015. The long noncoding RNA *lncTCF7* promotes self-renewal of human liver cancer stem cells through activation of Wnt signaling. Cell Stem Cell 16, 413–425.

Wen, X.J., Ding, Y., Tan, Z., Wang, J.X., Zhang, D., Wang, Y.C., 2020. Identification and characterization of cadmium stress-related LncRNAs from *Betula platyphylla*. Plant Sci. 299, 110601.

Wierzbicka, M., Potocka, A., 2002. Lead tolerance in plants growing on dry and moist soils. Acta Biol. Cracov. Ser. Bot. 44, 21–28.

Xu, Y., Wu, D., Liu, J., Huang, S., Zuo, Q., Xia, X., Jiang, Y., Wang, S., Chen, Y., Wang, T., Sun, L., 2018. Downregulated lncRNA *HOXA11-AS* affects trophoblast cell proliferation and migration by regulating *RND3* and *HOXA7* expression in PE. Mol. Ther. Nucleic Acids 12, 195–206.

Xu, Y.F., Zhou, G.K., Zhou, L., Li, Y.Q., Liu, J.Y., 2007. Expression patterns of the rice class I metallothionein gene family in response to lead stress in rice seedlings and functional complementation of its members in lead-sensitive yeast cells. Chin. Sci. Bull. 52, 2203–2209.

Xue, W.J., 2020. The Mechanism of Citric Acid Inhibiting Cadmium Absorption and Transport in Rice. Chinese Academy of Agricultural Sciences,, Beijing, China.

Yan, J., Wang, P., Wang, B., Hsu, C.C., Tang, K., Zhang, H., Hou, Y.J., Zhao, Y., Wang, Q., Zhao, C., Zhu, X., Tao, W.A., Li, J., Zhu, J.K., 2017. The SnRK2 kinases modulate miRNA accumulation in *Arabidopsis*. PLoS Genet. 13, e1006753.

Yao, B., Gu, X., Shu, Y.G., et al., 2019. Degradation of atrazine and changes in soil biological indices throughout dendroremediation using poplars. J. . Res. 30, 9.

Yu, G., Ma, J.C., Jiang, P.P., Li, J.Y., Gao, J.Y., Qiao, S.X., Zhao, Z.Y., 2019. The mechanism of plant resistance to heavy metal. IOP Conf. Ser. Earth Environ. Sci. 310, 052004.

Yu, Y., 2011. The Effects of Lead Stress on the Biochemical Characteristics and the Organization of Microtubule Cytoskeleton in Three Poplars. Beijing Forestry University,, Beijing, China.

Zhan, H.Y., Jiang, Y.F., Yuan, J., Hu, X.F., Nartey, O.D., Wang, B.L., 2014. Trace metal pollution in soil and wild plants from lead–zinc smelting areas in Huixian County, Northwest China. J. Geochem Explor 147, 182–188.

Zhang, X., Wang, W., Zhu, W., Dong, J., Cheng, Y., Yin, Z., Shen, F., 2019. Mechanisms and functions of long non-coding RNAs at multiple regulatory levels. Int. J. Mol. Sci. 20, 5573.